Increased expression of Translocator protein (TSPO) marks pro-inflammatory microglia but does not predict neurodegeneration

Lien Beckers[1], Dieter Ory[2]*, Ivana Geric[1], Lieven Declercq[2], Michel Koole[3], Michael Kassiou[4], Guy Bormans[2$], Myriam Baes[1$]*

[1]KU Leuven - University of Leuven, Department of Pharmaceutical and Pharmacological Sciences, Cell Metabolism, Leuven, Belgium; [2]KU Leuven - University of Leuven, Department of Pharmaceutical and Pharmacological Sciences, Laboratory for Radiopharmacy, Leuven, Belgium; [3]KU Leuven-University of Leuven, Department of Nuclear Medicine and Molecular Imaging, Leuven, Belgium;
[4] School of Chemistry, The University of Sydney, NSW 2006, Australia
*equal first authors
$equal last authors

Short title: TSPO in pro-inflammatory non-neurodegenerative microglia

Corresponding author:

Myriam Baes, PhD
Laboratory for Cell Metabolism
Department of Pharmaceutical and Pharmacological Sciences
Campus Gasthuisberg O/N2
Herestraat 49
B 3000 Leuven
Tel + 32 16 330853
Fax + 32 16 330856
e-mail : Myriam.Baes@kuleuven.be

ABSTRACT

Purpose: Activation of the innate immune system plays a significant role in pathologies of the central nervous system (CNS). In order to follow disease progression and evaluate effectiveness of potential treatments involved in neuroinflammation, it is important to track neuroinflammatory markers *in vivo* longitudinally. The translocator protein (TSPO) is used as a target to image neuroinflammation as its expression is upregulated in reactive glial cells during CNS pathologies. However, it remains unclear in which microglial phenotypes TSPO levels are upregulated, as microglia can display a plethora of activation states that can be protective or detrimental to the CNS.

Procedures: We assessed the levels of TSPO transcripts in cultured microglia that were polarized into pro- and anti-inflammatory states *in vitro* and in the brain of mice in which an anti-inflammatory environment was induced *in vivo.* In addition, we used a mouse model of peroxisomal multifunctional protein-2 (MFP2) deficiency that exhibits widespread neuroinflammation despite no neuronal loss and monitored TSPO expression by immunohistochemistry and by imaging using the TSPO radiotracer [^{18}F]DPA-714.

Results: TSPO expression was selectively increased in so-called classically activated or M1 microglia but not in alternatively activated or M2 microglia *in vitro*. In agreement, TSPO transcript levels were not induced in an anti-inflammatory brain environment. We found that both transcript and protein levels of TSPO are significantly increased in the brain of *Mfp2*$^{-/-}$ compared to control mice and TSPO immunoreactivity colocalized predominantly with microglia in *Mfp2*$^{-/-}$ brain. *In vitro* and *ex vivo* autoradiography in *Mfp2*$^{-/-}$ mice using the TSPO radiotracer [^{18}F]DPA-714, confirmed increased expression of TSPO. These data demonstrate that TSPO imaging reveals microgliosis in non-neurodegenerative brain pathologies.

Conclusions: We show that induced TSPO expression marks a pro-inflammatory brain environment that is not necessarily accompanied by neuronal loss.

Keywords

TSPO, neuro-inflammation, microglia, PET tracer, peroxisomes, mouse model

INTRODUCTION

The innate immune system is implicated in all neurodegenerative disorders. Key players in neuroinflammatory processes are microglia and astrocytes. They become reactive, typically change their morphology and acquire modified functions [1, 2]. Neuroinflammation often precedes neuronal loss in neurodegenerative disorders such as in Alzheimer's disease (AD) and Parkinson's disease (PD) [3, 4]. Therefore, it is important to detect neuroinflammatory processes in presymptomatic stages as they mark early stages of neuropathology. The most studied biomarker for imaging of neuroinflammation is the 18 kDa translocator protein (TSPO), previously known as the peripheral benzodiazepine receptor (PBR), which is primarily expressed on the outer mitochondrial membrane of microglia and macrophages [5, 6]. TSPO is important for brain development and homeostasis during adulthood as it plays a crucial role in neurosteroidogenesis [7, 8]. TSPO expression in the CNS is low under healthy circumstances, but increases mainly in microglia in response to neuronal insults such as in the neurodegenerative diseases PD, AD, Amyotrophic lateral sclerosis (ALS), and Huntington disease (HD) [9, 10]. Reactive astrocytes can also induce TSPO expression in addition to reactive microglia [11].

It is still a matter of debate whether neuroinflammation accelerates or delays disease progression in neurological disorders. Reactive microglia play Janus-like roles in neurological disorders. During pathology, activated microglia can promote tissue injury (denoted as an M1 phenotype) but also tissue repair and remodelling (denoted as an M2 phenotype), dependent on type of disease and stage of disease progression [12, 13]. Therefore, it is important to precisely characterise neuroinflammation *in vivo* in order to apply anti-inflammatory therapies only during harmful functioning of the innate immune system. Although TSPO is generally accepted as an appropriate marker of neuroinflammation, the functional link between TSPO and neuroinflammation remains unknown. It is unclear whether increased TSPO expression is associated with pro-inflammatory and neurotoxic responses (classically activated or M1 microglia), or with anti-inflammatory responses and tissue repair (alternatively activated or M2 microglia), or both. Whereas the association of TSPO with specific inflammatory states is poorly documented [14], this information is necessary to correctly interpret increased TSPO levels *in vivo* in clinical conditions and to adapt inflammatory therapies according to the need and disease stage of patients.

In this study, we aimed to better define in which neuroinflammatory conditions TSPO is induced. First, microglia were isolated from wild type brain and TSPO transcript expression was analyzed after polarization of the microglia into a pro- or anti-inflammatory state. This was complemented by an *in vivo* study in which an anti-inflammatory brain environment was created by intracerebroventricular (i.c.v.) injection of IL-4. In addition, we used a mouse model of peroxisomal β-oxidation deficiency, more specifically multifunctional protein-2 (MFP2) deficient mice, which develop robust and chronic neuroinflammation before the age of 8 weeks that progressively increases until death around the age of 17 weeks [15-17]. The mechanisms underlying this widespread gliosis were not elucidated yet but likely an interplay of cell-autonomous deregulation due to loss of MFP2 in microglia and microglial reactivity to neuronal dysfunction are involved [15,16]. Different from most other neuropathological disease models in which neuroinflammation develops, *Mfp2*$^{-/-}$ mice do not show neuronal loss [17]. We previously characterized the proliferative *Mfp2*$^{-/-}$ microglia extensively and found that they are of local origin, are immunologically activated but display a mixed pro- (M1) and anti- (M2) inflammatory phenotype [17]. Of note, they do not express detrimental neuroinflammatory markers such as iNOS. We investigated whether TSPO is induced in this inflamed but non-neurodegenerative brain environment by immunohistological and gene expression studies and by *in vitro*, *ex vivo* and *in vivo* TSPO imaging using the TSPO specific radiotracer [^{18}F]DPA-714.

MATERIALS AND METHODS

Mouse breeding

Mfp2$^{-/-}$ mice were generated as previously described [18]. *Mfp2*$^{-/-}$ mice were bred on a Swiss/Webster background in a specific pathogen free animal housing facility of the KU Leuven, had *ad libitum* access to water and standard rodent food, and were kept on a 12-hour light and dark cycle. All animal experiments were performed in accordance with the "Guidelines for Care and Use of Experimental Animals" and fully approved by the Research Ethical committee of the KU Leuven (#190/2012). Both wild type and heterozygous mice were used as controls as no differences were detected in our previous investigations [15-17].

Immunohistochemistry

Anesthesia of the mice and tissue processing for immunohistochemical (IHC) staining were performed as described [19]. Paraffin sections (7 µm) were used for immunofluorescent staining. The following primary antibodies were used: polyclonal rabbit anti-Iba1 (1:500; Wako D19-19741), rabbit anti-PBR (TSPO) (1:100; Abcam ab109497), rabbit anti-GFAP (1:200; Sigma G9269). After overnight incubation with primary antibodies at room temperature, HRP-labeled secondary antibodies (1:200) were applied for 1 hour, followed by fluorescent labeling with a cyanine 2 (FITC) TSA kit (Perkin Elmer Life sciences, Boston, USA). When double immunolabeling was performed, sets of primary and secondary antibodies were applied sequentially. The cyanine 3 TSA kit (Perkin Elmer Life sciences) was used as second fluorescent label. Images were acquired with a motorized inverted IX-81 microscope connected to a CCD-FV2T digital camera (Olympus, Aartselaar, Belgium) and processed with LSM Image browser software (Zeiss, Germany).

Quantitative real time (qRT-)PCR

RNA was extracted from cultured microglia using the PureLink RNA Mini Kit according to the manufacturer's protocol and converted to cDNA using the Qiagen QuantiTect Reverse Transcription Kit. RNA was isolated from frontal cortex by using Trizol extraction following the manufacturer's instructions (Thermofisher).

Real time PCR was performed as previously described [20] using an ABI PRISM 7500 Real Time PCR instrument (Applied Biosystems, Lennik, Belgium). Sets of validated primers and probes were ordered from Integrated DNA Technologies (IDT, Leuven, Belgium) or from Applied Biosystems (primer and probe sequences are listed in Suppl. Table 1). Assays were performed in triplicate in 10 µL TaqMan Fast Universal PCR Master Mix (Applied Biosystems). Relative expression levels of the target genes were calculated taking into account the amplification efficiency as described [21]. The relative expression levels of the target genes were calculated as a ratio to the housekeeping gene β-actin. Statistics were carried out using Graphpad Prism v5.0 software (San Diego, CA).

Primary microglial cell culture

For the preparation of primary microglia cultures, control mice from C57BL6/J background were used. The cultures were derived from the cortices of mice at postnatal day 0-1 as previously described [22]. Briefly, mice where decapitated and cortices dissected. After removal of the meninges, cortices were mechanically dissociated and the cell suspension was diluted with low glucose DMEM supplemented with 10% fetal bovine serum and 0.01% penicillin-streptomycin and cultured in T75 flasks. At day 14 *in vitro* microglia cells were isolated by shaking and rinsing the flasks. The purity of obtained cultures was confirmed by Cd11b flow-cytometry and found to be higher than 95% (Suppl. Fig 1).

For RNA isolation microglia cells were plated in a 12-well plate at a density of 500 000 cells/well. One day after plating, cells were stimulated for 24h with vehicle (PBS 10 µl/ml), lipopolysaccharides (LPS) (1 µg/ml, Sigma Aldrich) or IL-1β/IFNγ (IL-1 β: 50 ng/ml; IFNγ: 20 ng/ml, R&D), or IL-4 (20 ng/ml, Sigma Aldrich) in order to shift them to the M0, M1 and M2 phenotype, respectively.

Intracerebroventricular injections

Male mice (15-16 weeks old) with a C57BL/6NTac background were used for i.c.v. injections with IL-4 as described previously [23]. Mice were anesthetized with ketamine and xylazine (100 and 10 mg/kg respectively) and injected with vehicle (0.9% NaCl) or 200 ng IL-4 (R&D) in a total volume of 2.5 µl in the third cerebral ventricle using the following stereotaxic coordinates: bregma, −0.25 mm; lateral, 1 mm; depth, 2.25 mm. The animals were allowed to recover for 20 h, after which they were sacrificed with an overdose of dormitor and nimatek (1 mg and 100 mg/kg, respectively). The frontal cortex contralateral to the injection site was collected and snap frozen in liquid nitrogen.

In vitro autoradiography

Mice (n=3/group) were sacrificed at an age of 19 weeks, brain was removed, rinsed with saline to remove blood, rapidly frozen in 2-methylbutane (-40 °C) and stored at -20 °C for 24 h. Brain sagittal sections were obtained using a cryotome (Shandon cryotome FSE; Thermo Fisher, Waltham, USA), mounted on adhesive microscope slides (Superfrost Plus; Thermo Fisher) and stored at -20 °C until autoradiography was performed. Brain slices were dried and pre-incubated in tris-HCl 50 mM buffer (pH 7.4) for 10 min at room temperature. Before incubation with [^{18}F]DPA-714, the brain sections were dried. The brain sections were incubated with 300 kBq (in 500 µL tris HCl 50 mM buffer) of tracer for 10 min or tracer in the presence of 20 µM of the blocking agent PK11195 (Sigma Aldrich, St. Louis, MO, USA) for 10 min. The brain sections were washed twice for 10 min in tris-HCl 50 mM (pH 7.4) and 0.3% BSA buffer at 4 °C. After a quick dip in water at 4 °C, the slides were dried. Autoradiograms were obtained by exposing the slides for 5 min to a high-performance phosphor storage screen (super-resolution screen; Perkin Elmer, Waltham, USA). The screens were read using a Cyclone Plus system (Perkin Elmer) and analyzed using Optiquant software (Perkin Elmer). The radioactivity concentration in the autoradiograms is expressed in digital light units (DLU)/mm², corrected for background. All statistical studies were performed with the unpaired two-tailed student t-test. Calculations were carried out using GraphPad Prism v5.0 (San Diego, CA).

Ex vivo autoradiography

Mice (16 weeks old, n=6/group) were injected with the tracer (22 ± 0.6 MBq, mean ± SD) via a tail vein under anesthesia (2.5% isoflurane in O2 at 1 L/min flow rate) and were kept under anesthesia until they were sacrificed by decapitation at 30 min (n=3/group) and 60 min (n=3/group) post tracer injection. Brain was removed and rapidly frozen in 2-methylbutane (between -30 °C and -40 °C). 20 µm sagittal sections from brain were obtained using a cryotome (Shandon cryotome FSE, Thermo Fisher, Waltham, USA), mounted on adhesive microscope slides (Superfrost Plus, Thermo Fisher Scientific) and exposed to a phosphor storage screen film (super resolution screen; Perkin Elmer, Downers Grove, IL, USA) for 35 min. The screens were read using a Cyclone® Plus system (Perkin Elmer) and analyzed using Optiquant software (Perkin Elmer). The results were expressed as DLU/mm^2 normalized for body weight of the animal and injected dose [(DLU/mm^2) * (body weight/injected dose)].

microPET

Imaging experiments were performed on a Focus 220 microPET scanner (Concorde Microsystems, Knoxville, TN, USA). Six *Mfp2*$^{-/-}$ (26.5 ± 2.7 g, mean ± SD) and six control mice (39.8 ± 5.9 g) were scanned at end stage of disease, between 14 and 19 weeks of age. Mice were injected with 22 ± 0.6 MBq (mean ± SD) of [^{18}F]DPA-714 via a tail vein (volume injected <0.3 mL). During all PET sessions, animals were kept under gas anesthesia (2.5% isoflurane in O_2 at a flow rate of 1 L/min). List-mode 90-min microPET scans were acquired. Acquisition data were then Fourier rebinned in 24 time frames (4 x 15 seconds (s), 4 x 60 s, 5 x 180 s, 8 x 300 s, 3 x 600 s) and reconstructed using maximum a posteriori iterative reconstruction. The images were spatially aligned to a rat brain [^{18}F]FDG template in Paxinos coordinates [24] using an affine transformation, allowing the use of a predefined volumes of interest map. Time-activity curves (TAC) were generated for total brain for each individual scan using PMOD software (version 3.2; PMOD technologies, Zurich, Switzerland).

RESULTS

Induced TSPO expression is restricted to classically (M1) activated microglia

It is known that activated microglia exert dual functions, either pro-inflammatory (M1) functions that are rather harmful, or anti-inflammatory (M2) functions that are neuroprotective and regenerative [25]. While this M1-M2 distinction is an oversimplification and represents the extreme states, this subdivision is a nice strategy to associate certain disease phenomena with a specific activation state of microglia. Although TSPO is a well-known marker for general neuroinflammation, it is still unknown whether TSPO expression is induced during both pro- and anti-inflammatory activation states of microglia or during a specific activation state only. In this study, we aimed to associate induced TSPO expression with either a pro-inflammatory (M1) or anti-inflammatory (M2) activation state of microglia. First, cultured primary microglia isolated from newborn wild-type mice were polarized into a pro-inflammatory phenotype by using either LPS or the combination of Interleukin (IL)-1β and Interferon gamma (IFNγ). Alternatively, they were brought into an anti-inflammatory state by treating with IL-4 [26-28]. We verified that LPS and IL-1β/IFNγ polarizes the microglia towards an M1 state by showing increased transcript expression of the pro-inflammatory markers *Tnfa* (Fig. 1a and Suppl. Fig. 2a) and *iNOS* (Fig. 1b and Suppl. Fig. 2b) compared to vehicle-treated (M0) microglia whereas the M2 marker arginase-1 *(Arg1)* remained barely detectable (Fig. 1c and Suppl. Fig. 2c). Successful polarization to the M2 state with IL-4 was shown by strongly increased arginase-1 *(Arg1)* expression (Fig. 1c) and levels of *iNOS* and *Tnfa* that were unaltered compared to the M0 condition [26]. We found that *Tspo* transcript expression was induced in both groups of M1-activated microglia but did not change in M2-activated microglia (Fig. 1d and Suppl. Fig. 2d). Subsequently, we questioned whether the selective induction of TSPO in pro-inflammatory microglia *in vitro* also occurred in neuro-inflammatory conditions *in vivo*. We and others previously showed that TSPO expression is increased in models in which pro-inflammatory microglia predominate [29-31]. To induce an anti-inflammatory brain environment, we injected Il-4 in the third ventricle as previously reported [23, 32]. The expression of *Tspo* as well as of pro- and anti-inflammatory markers was assessed 20h later in the frontal cortex [23, 32]. As expected, the overall profile of inflammatory markers coincided rather with an anti-inflammatory than with a pro-inflammatory state (Fig. 2a-g). In this particular condition, in which neuro-inflammation was clearly established, expression of *Tspo* transcripts were unaltered (Fig. 2h).

Together, these data demonstrate that *Tspo* expression is not induced in all inflammatory brain environments but rather marks a pro-inflammatory state.

TSPO transcript and protein levels are induced in *Mfp2*$^{-/-}$ brain

We previously demonstrated that in MFP2-deficient brain a robust and chronic neuroinflammation develops that is not accompanied by overt loss of neurons [17]. In order to analyse whether TSPO expression is increased in the CNS of *Mfp2*$^{-/-}$ mice, we first examined the transcript levels. Quantitative RT-PCR showed increased *Tspo* mRNA in brainstem of *Mfp2*$^{-/-}$ mice as compared to control mice at an age of 12 weeks (Fig. 3a). To ascertain that increased transcript levels are translated at the protein level, IHC was performed. Whereas TSPO immunoreactivity was hardly detectable in healthy control brain, TSPO was easily visualized throughout the whole *Mfp2*$^{-/-}$ brain (shown for brainstem, colliculus and thalamus in Fig. 3b-g).

Upregulated TSPO colocalizes predominantly with reactive microglia in *Mfp2*$^{-/-}$ brain

Increased TSPO expression was generally considered to be dedicated to microglia, but recent literature suggests a potential contribution of reactive astrocytes [11, 33, 34]. In order to assess whether microglia, astrocytes or both contribute to increased TSPO levels in *Mfp2*$^{-/-}$ brain, IHC staining of TSPO protein with cell type-specific markers (Iba1 for microglia and GFAP for astrocytes) was performed. Nearly all Iba1^{+} microglia express TSPO in *Mfp2*$^{-/-}$ brain (shown for colliculus in Fig. 3i) whereas only few GFAP^{+} astrocytes show TSPO expression (marked by arrows, Fig. 3k), indicating that increased TSPO levels are mainly attributed to reactive microglia in the *Mfp2*$^{-/-}$ brain.

Increased [^{18}F]DPA-714 uptake in *Mfp2*$^{-/-}$ brain: *In vitro* assessment of brain TSPO levels

In order to evaluate whether increased expression of TSPO in *Mfp2*$^{-/-}$ brain could also be detected by using radiolabeled ligands for this protein, *in vitro* autoradiography employing [^{18}F]DPA-714, an established PET tracer for TSPO, was used in a first approach. The results showed significantly higher tracer binding in the *Mfp2*$^{-/-}$ brain as compared to age-matched control brain ($P < 0.0001$; Fig. 4a,b). More specifically, high binding of [^{18}F]DPA-714 was observed in colliculus, brainstem, corpus callosum and hippocampus mirroring the immunofluorescent detection of TSPO (Fig. 4a). We performed a blocking study using PK11195 (20 µM) as a blocking agent on brain slices of *Mfp2*$^{-/-}$ mice. PK11195

significantly reduced [^{18}F]DPA-714 binding (P<0.0001; Fig. 4c), demonstrating TSPO-specific binding of [^{18}F]DPA-714.

Increased [^{18}F]DPA-714 uptake in *Mfp2*$^{-/-}$ brain: *Ex vivo* assessment of brain TSPO levels

Ex-vivo autoradiography was used to verify whether the increased TSPO expression observed *in vitro* is sufficient to be detected after intravenous injection of [^{18}F]DPA-714. *Ex-vivo* autoradiography has a 10-fold higher resolution than microPET and is therefore more sensitive to reveal increased tracer concentration in small brain areas. Analysis of the *ex vivo* autoradiography data showed significantly higher tracer binding in the *Mfp2*$^{-/-}$ brain as compared to the age-matched control brain both at 30 min (P = 0.0017) and 60 min (P < 0.0001) after [^{18}F]DPA-714 injection (Fig. 4d-g).

MicroPET: *In vivo* assessment of brain TSPO levels

Although the resolution of the microPET scanner (1.4 mm FWHM in the centre) is low relative to the brain size of mice so that partial volume effects may obscure increase of tracer binding in small brain areas, we explored whether we would be able to detect increased [^{18}F]DPA-714 binding *in vivo* in *Mfp2*$^{-/-}$ mice compared to control mice. Figure 5 shows the TACs and brain images of the microPET scan of *Mfp2*$^{-/-}$ mice and age-matched control mice. The TAC expressed as nCi/cc of [^{18}F]DPA-714 and accompanying brain images shows slower wash out for *Mfp2*$^{-/-}$ mice compared with that of controls (Fig. 5a,c) in line with the *ex vivo* autoradiography findings. When the TAC is expressed as standard uptake (SUV) value, the initial brain uptake is clearly lower for *Mfp2*$^{-/-}$ mice compared to control mice, whereas clearance rate from brain is slower for *Mfp2*$^{-/-}$ mice (Fig. 5b,d).

DISCUSSION

Microglia can perform a multitude of tasks in the CNS depending on physiological – pathological conditions and adapt their gene expression profile accordingly. Although TSPO has been widely used as a reactive microglia-specific neuroinflammation imaging target [35-37], it is unclear which microglial phenotypes are actually visualized [14]. By using *in vitro* and *in vivo* approaches, we demonstrate that TSPO is upregulated in pro-inflammatory microglia that, however, not necessarily reside in a destructive brain milieu.

In vitro, microglia can be manipulated and skewed into two extreme states, analogous to macrophages. The described M1 - M2 subdivision nicely reflects the Janus-like behavior of microglia regarding their promotion of either tissue injury (M1) or repair (M2), but it is an oversimplified concept and only represents extreme states [38]. We show in this study that transcript levels of TSPO only increase in pro-inflammatory (M1) and not in anti-inflammatory (M2) microglial cells. Although this suggests that TSPO rather marks a harmful inflammatory brain environment and that TSPO is not induced in a purely neuroprotective or regenerative brain environment, this needs to be translated *in vivo*. There are several examples of neuro-inflammatory conditions in which pro-inflammatory microglia prevail in which it was shown that TSPO is upregulated [29-31]. By i.c.v. injection of IL-4 we now elicited neuro-inflammation that was primarily characterized by increased expression of anti-inflammatory markers. In this particular neuro-inflammatory state, the expression of TSPO was unchanged, further proving that by tracking TSPO only a subset of neuro-inflammatory cells are revealed. Although microglia with either a pro- or anti-inflammatory signature can occur in defined pathological conditions [27], it is now accepted that microglia *in vivo* mostly adopt mixed pro- and anti-inflammatory phenotypes in neurological disorders [17, 38, 39]. It will be important to corroborate our findings in neurological disease states in which the microglial phenotypes have been well characterized. For example, in a mouse model of ALS it was shown that M2 microglia are abundant in the early phase, whereas M1 microglia dominate at end stage of disease [40].

This study also demonstrates that TSPO levels are clearly induced *in vivo* in a mouse model of peroxisomal MFP2 deficiency that develops robust neuroinflammation [17]. The results from IHC staining were confirmed by *in vitro* and *ex vivo* autoradiography with [^{18}F]DPA-714 demonstrating increased TSPO-specific binding in several brain areas of *Mfp2*$^{-/-}$ mice in comparison with control

mice. The *in vivo* PET imaging data were more difficult to interpret probably due to the limited resolution of our micro PET scanner, although tracer clearance rate from the brain of *Mfp2*$^{-/-}$ mice was slower compared to control mice as was clearly demonstrated by both the nCi/cc and SUV curves. This is indicative for a higher target expression in brain tissue of *Mfp2*$^{-/-}$ mice, but a higher tracer metabolism rate cannot be excluded. The difference between nCi/cc and SUV curves can be explained by a different brain-to-total-body mass ratio for *Mfp2*$^{-/-}$ versus control mice which influences the SUV values. *Mfp2*$^{-/-}$ mice are generally 25% smaller than control mice [41].

The cellular and molecular characteristics of the inflammatory response in *Mfp2*$^{-/-}$ mice were previously extensively characterized [17]. It is noteworthy that the massive increase in myeloid cells was not due to infiltration of peripheral monocytes. Furthermore, the microenvironment in *Mfp2*$^{-/-}$ brain deviates from the milieu in neurodegenerative disorders as there is neither neuronal loss nor oxidative stress during the entire lifespan of *Mfp2*$^{-/-}$ mice despite the robust neuroinflammatory response [17]. Although the expanded microglia population expressed mixed pro- and anti-inflammatory markers, it should be noted that *Mfp2*$^{-/-}$ microglia do not upregulate neurotoxic and oxidative stress markers such as Nos2, Il6 and Icam1 [16, 17]. Thus, our data reveal that TSPO labels pro-inflammatory microglia that do not have a neuro-destructive character.

In some but not all neuroinflammatory models, TSPO was shown to be upregulated in astrocytes in addition to microglia [6, 11, 42, 43]. In the *Mfp2*$^{-/-}$ brain, only a minority of astrocytes showed elevated TSPO levels, which is in contrast to microglia that virtually all induce TSPO. This supports the hypothesis that transition of resident microglia, and not astrocytes [44], from a resting to an activated phenotype principally underlies the increased TSPO expression.

Taken together, the *in vitro* data showing that TSPO expression is not increased in anti-inflammatory circumstances supports its use as a marker for pro-inflammatory microglia imaging. However, TSPO upregulation does not distinguish whether microglia develop a neuro-destructive signature or not. An additional caveat regarding TSPO is that a human TSPO polymorphism with a trimodal distribution in binding affinity (high-affinity, low-affinity and mixed affinity binders) was uncovered for several TSPO ligands [45]. This implicates that knowledge of binding status is needed to correctly quantify TSPO expression using these PET ligands in humans [45]. Also the fact that the particular function of TSPO in mounting the inflammatory response remains obscure, is a drawback for its use as a biomarker.

Therefore, it is highly desirable to identify new targets that allow specific visualization of neurotoxic microglia. P2X7, for which versatile radiotracers were already developed, might be a good marker besides other candidates [46, 47]. In addition, in view of the therapeutic potential to convert pro-inflammatory into anti-inflammatory microglia [27], there is also a need to selectively detect the latter microglia by *in vivo* imaging in order to assess the therapeutic benefit. Given the ill-defined molecular phenotype of healing microglia [27], this will be a more difficult task.

ACKNOWLEDGMENTS

The authors wish to thank Benno Das, Lies Pauwels, Julie Cornelis, and Ann Bouché for their excellent technical assistance. This work was funded by grants from Fonds Wetenschappelijk Onderzoek Vlaanderen (G.0675.12 and G.0A15.13), KU Leuven (OT12/78), European Union's Seventh Framework Programme [FP7/2007-2013], INMiND (Grant agreement no. 278850) and Programme financing KU Leuven IMIR.

Conflict of Interest: The authors declare that they have no conflict of interest.

REFERENCES

[1] K. Saijo, C.K. Glass, Microglial cell origin and phenotypes in health and disease, Nat Rev Immunol, 11 (2011) 775-787.

[2] D. Gomez-Nicola, N.L. Fransen, S. Suzzi, V.H. Perry, Regulation of microglial proliferation during chronic neurodegeneration, J Neurosci, 33 (2013) 2481-2493.

[3] M.T. Heneka, M.J. Carson, J. El Khoury, G.E. Landreth, F. Brosseron, D.L. Feinstein, A.H. Jacobs, T. Wyss-Coray, J. Vitorica, R.M. Ransohoff, K. Herrup, S.A. Frautschy, B. Finsen, G.C. Brown, A. Verkhratsky, K. Yamanaka, J. Koistinaho, E. Latz, A. Halle, G.C. Petzold, T. Town, D. Morgan, M.L. Shinohara, V.H. Perry, C. Holmes, N.G. Bazan, D.J. Brooks, S. Hunot, B. Joseph, N. Deigendesch, O. Garaschuk, E. Boddeke, C.A. Dinarello, J.C. Breitner, G.M. Cole, D.T. Golenbock, M.P. Kummer, Neuroinflammation in Alzheimer's disease, Lancet Neurol, 14 (2015) 388-405.

[4] E.C. Hirsch, S. Hunot, Neuroinflammation in Parkinson's disease: a target for neuroprotection?, Lancet Neurol, 8 (2009) 382-397.

[5] M.K. Chen, T.R. Guilarte, Translocator protein 18 kDa (TSPO): molecular sensor of brain injury and repair, Pharmacol Ther, 118 (2008) 1-17.

[6] M. Cosenza-Nashat, M.L. Zhao, H.S. Suh, J. Morgan, R. Natividad, S. Morgello, S.C. Lee, Expression of the translocator protein of 18 kDa by microglia, macrophages and astrocytes based on immunohistochemical localization in abnormal human brain, Neuropathol Appl Neurobiol, 35 (2009) 306-328.

[7] J. Fan, E. Campioli, A. Midzak, M. Culty, V. Papadopoulos, Conditional steroidogenic cell-targeted deletion of TSPO unveils a crucial role in viability and hormone-dependent steroid formation, Proc Natl Acad Sci U S A, 112 (2015) 7261-7266.

[8] J.J. Lacapere, V. Papadopoulos, Peripheral-type benzodiazepine receptor: structure and function of a cholesterol-binding protein in steroid and bile acid biosynthesis, Steroids, 68 (2003) 569-585.

[9] R. Rupprecht, V. Papadopoulos, G. Rammes, T.C. Baghai, J. Fan, N. Akula, G. Groyer, D. Adams, M. Schumacher, Translocator protein (18 kDa) (TSPO) as a therapeutic target for neurological and psychiatric disorders, Nat Rev Drug Discov, 9 (2010) 971-988.

[10] D. Ory, S. Celen, A. Verbruggen, G. Bormans, PET radioligands for in vivo visualization of neuroinflammation, Curr Pharm Des, 20 (2014) 5897-5913.

[11] S. Lavisse, M. Guillermier, A.S. Herard, F. Petit, M. Delahaye, N. Van Camp, L. Ben Haim, V. Lebon, P. Remy, F. Dolle, T. Delzescaux, G. Bonvento, P. Hantraye, C. Escartin, Reactive astrocytes overexpress TSPO and are detected by TSPO positron emission tomography imaging, J Neurosci, 32 (2012) 10809-10818.

[12] T. Wyss-Coray, L. Mucke, Inflammation in neurodegenerative disease--a double-edged sword, Neuron, 35 (2002) 419-432.

[13] R.M. Ransohoff, How neuroinflammation contributes to neurodegeneration, Science, 353 (2016) 777-783.

[14] S.A. Wolf, H.W. Boddeke, H. Kettenmann, Microglia in Physiology and Disease, Annu Rev Physiol, (2016).

[15] S. Huyghe, H. Schmalbruch, L. Hulshagen, P.V. Veldhoven, M. Baes, D. Hartmann, Peroxisomal multifunctional protein-2 deficiency causes motor deficits and glial lesions in the adult central nervous system, Am J Pathol, 168 (2006) 1321-1334.

[16] S. Verheijden, A. Bottelbergs, O. Krysko, D.V. Krysko, L. Beckers, S. De Munter, P.P. Van Veldhoven, S. Wyns, W. Kulik, K.A. Nave, M.S. Ramer, P. Carmeliet, C.M. Kassmann, M. Baes, Peroxisomal multifunctional protein-2 deficiency causes neuroinflammation and degeneration of Purkinje cells independent of very long chain fatty acid accumulation, Neurobiol Dis, 58 (2013) 258-269.

[17] S. Verheijden, L. Beckers, A. Casazza, O. Butovsky, M. Mazzone, M. Baes, Identification of a chronic non-neurodegenerative microglia activation state in a mouse model of peroxisomal beta-oxidation deficiency, Glia, 63 (2015) 1606-1620.
[18] M. Baes, S. Huyghe, P. Carmeliet, P.E. Declercq, D. Collen, G.P. Mannaerts, P.P. Van Veldhoven, Inactivation of the peroxisomal multifunctional protein-2 in mice impedes the degradation of not only 2-methyl-branched fatty acids and bile acid intermediates but also of very long chain fatty acids, J Biol Chem, 275 (2000) 16329-16336.
[19] L. Hulshagen, O. Krysko, A. Bottelbergs, S. Huyghe, R. Klein, P.P. Van Veldhoven, P.P. De Deyn, R. D'Hooge, D. Hartmann, M. Baes, Absence of functional peroxisomes from mouse CNS causes dysmyelination and axon degeneration, J Neurosci, 28 (2008) 4015-4027.
[20] A. Bottelbergs, S. Verheijden, L. Hulshagen, D.H. Gutmann, S. Goebbels, K.A. Nave, C. Kassmann, M. Baes, Axonal integrity in the absence of functional peroxisomes from projection neurons and astrocytes, Glia, 58 (2010) 1532-1543.
[21] A. Giulietti, L. Overbergh, D. Valckx, B. Decallonne, R. Bouillon, C. Mathieu, An overview of real-time quantitative PCR: applications to quantify cytokine gene expression, Methods, 25 (2001) 386-401.
[22] V. Chhor, T. Le Charpentier, S. Lebon, M.V. Ore, I.L. Celador, J. Josserand, V. Degos, E. Jacotot, H. Hagberg, K. Savman, C. Mallard, P. Gressens, B. Fleiss, Characterization of phenotype markers and neuronotoxic potential of polarised primary microglia in vitro, Brain Behav Immun, 32 (2013) 70-85.
[23] G. Pepe, G. Calderazzi, M. De Maglie, A.M. Villa, E. Vegeto, Heterogeneous induction of microglia M2a phenotype by central administration of interleukin-4, J Neuroinflammation, 11 (2014) 211.
[24] C. Casteels, P. Vermaelen, J. Nuyts, A. Van Der Linden, V. Baekelandt, L. Mortelmans, G. Bormans, K. Van Laere, Construction and evaluation of multitracer small-animal PET probabilistic atlases for voxel-based functional mapping of the rat brain, J Nucl Med, 47 (2006) 1858-1866.
[25] D. Boche, V.H. Perry, J.A. Nicoll, Review: activation patterns of microglia and their identification in the human brain, Neuropathol Appl Neurobiol, 39 (2013) 3-18.
[26] A. Mantovani, S.K. Biswas, M.R. Galdiero, A. Sica, M. Locati, Macrophage plasticity and polarization in tissue repair and remodelling, J Pathol, 229 (2013) 176-185.
[27] J.D. Cherry, J.A. Olschowka, M.K. O'Banion, Neuroinflammation and M2 microglia: the good, the bad, and the inflamed, J Neuroinflammation, 11 (2014) 98.
[28] R. Orihuela, C.A. McPherson, G.J. Harry, Microglial M1/M2 polarization and metabolic states, Br J Pharmacol, 173 (2016) 649-665.
[29] D. Ory, A. Planas, T. Dresselaers, W. Gsell, A. Postnov, S. Celen, C. Casteels, U. Himmelreich, Z. Debyser, K. Van Laere, A. Verbruggen, G. Bormans, PET imaging of TSPO in a rat model of local neuroinflammation induced by intracerebral injection of lipopolysaccharide, Nucl Med Biol, 42 (2015) 753-761.
[30] D. Ory, A. Postnov, M. Koole, S. Celen, B. de Laat, A. Verbruggen, K. Van Laere, G. Bormans, C. Casteels, Quantification of TSPO overexpression in a rat model of local neuroinflammation induced by intracerebral injection of LPS by the use of [(18)F]DPA-714 PET, Eur J Nucl Med Mol Imaging, 43 (2016) 163-172.
[31] R. Scholz, M. Sobotka, A. Caramoy, T. Stempfl, C. Moehle, T. Langmann, Minocycline counter-regulates pro-inflammatory microglia responses in the retina and protects from degeneration, J Neuroinflammation, 12 (2015) 209.
[32] S. Girard, D. Brough, G. Lopez-Castejon, J. Giles, N.J. Rothwell, S.M. Allan, Microglia and macrophages differentially modulate cell death after brain injury caused by oxygen-glucose deprivation in organotypic brain slices, Glia, 61 (2013) 813-824.
[33] S. Rojas, A. Martin, M.J. Arranz, D. Pareto, J. Purroy, E. Verdaguer, J. Llop, V. Gomez, J.D. Gispert, O. Millan, A. Chamorro, A.M. Planas, Imaging brain inflammation with [(11)C]PK11195 by PET and induction of the peripheral-type benzodiazepine receptor after transient focal ischemia in rats, J Cereb Blood Flow Metab, 27 (2007) 1975-1986.
[34] B. Ji, J. Maeda, M. Sawada, M. Ono, T. Okauchi, M. Inaji, M.R. Zhang, K. Suzuki, K. Ando, M. Staufenbiel, J.Q. Trojanowski, V.M. Lee, M. Higuchi, T. Suhara, Imaging of peripheral benzodiazepine

receptor expression as biomarkers of detrimental versus beneficial glial responses in mouse models of Alzheimer's and other CNS pathologies, J Neurosci, 28 (2008) 12255-12267.
[35] P. Corcia, C. Tauber, J. Vercoullie, N. Arlicot, C. Prunier, J. Praline, G. Nicolas, Y. Venel, C. Hommet, J.L. Baulieu, J.P. Cottier, C. Roussel, M. Kassiou, D. Guilloteau, M.J. Ribeiro, Molecular imaging of microglial activation in amyotrophic lateral sclerosis, PloS one, 7 (2012) e52941.
[36] W.C. Kreisl, C.H. Lyoo, M. McGwier, J. Snow, K.J. Jenko, N. Kimura, W. Corona, C.L. Morse, S.S. Zoghbi, V.W. Pike, F.J. McMahon, R.S. Turner, R.B. Innis, P.E.T.R.P.T. Biomarkers Consortium, In vivo radioligand binding to translocator protein correlates with severity of Alzheimer's disease, Brain, 136 (2013) 2228-2238.
[37] E. Harberts, D. Datta, S. Chen, J.E. Wohler, U. Oh, S. Jacobson, Translocator protein 18 kDa (TSPO) expression in multiple sclerosis patients, J Neuroimmune Pharmacol, 8 (2013) 51-57.
[38] R.M. Ransohoff, A polarizing question: do M1 and M2 microglia exist?, Nat Neurosci, 19 (2016) 987-991.
[39] D. Farfara, V. Lifshitz, D. Frenkel, Neuroprotective and neurotoxic properties of glial cells in the pathogenesis of Alzheimer's disease, J Cell Mol Med, 12 (2008) 762-780.
[40] B. Liao, W. Zhao, D.R. Beers, J.S. Henkel, S.H. Appel, Transformation from a neuroprotective to a neurotoxic microglial phenotype in a mouse model of ALS, Exp Neurol, 237 (2012) 147-152.
[41] S. Huyghe, H. Schmalbruch, K. De Gendt, G. Verhoeven, F. Guillou, P.P. Van Veldhoven, M. Baes, Peroxisomal multifunctional protein 2 is essential for lipid homeostasis in Sertoli cells and male fertility in mice, Endocrinology, 147 (2006) 2228-2236.
[42] E. Vlodavsky, J.F. Soustiel, Immunohistochemical expression of peripheral benzodiazepine receptors in human astrocytomas and its correlation with grade of malignancy, proliferation, apoptosis and survival, J Neurooncol, 81 (2007) 1-7.
[43] N. Mirzaei, S.P. Tang, S. Ashworth, C. Coello, C. Plisson, J. Passchier, V. Selvaraj, R.J. Tyacke, D.J. Nutt, M. Sastre, In vivo imaging of microglial activation by positron emission tomography with [(11)C]PBR28 in the 5XFAD model of Alzheimer's disease, Glia, 64 (2016) 993-1006.
[44] M. Politis, P. Su, P. Piccini, Imaging of microglia in patients with neurodegenerative disorders, Front Pharmacol, 3 (2012) 96.
[45] D.R. Owen, A.J. Yeo, R.N. Gunn, K. Song, G. Wadsworth, A. Lewis, C. Rhodes, D.J. Pulford, I. Bennacef, C.A. Parker, P.L. StJean, L.R. Cardon, V.E. Mooser, P.M. Matthews, E.A. Rabiner, J.P. Rubio, An 18-kDa translocator protein (TSPO) polymorphism explains differences in binding affinity of the PET radioligand PBR28, J Cereb Blood Flow Metab, 32 (2012) 1-5.
[46] D. Ory, S. Celen, R. Gijsbers, C. Van Den Haute, A. Postnov, M. Koole, C. Vandeputte, J.I. Andres, J. Alcazar, M. De Angelis, X. Langlois, A. Bhattacharya, M. Schmidt, M.A. Letavic, W. Vanduffel, K. Van Laere, A. Verbruggen, Z. Debyser, G. Bormans, Preclinical Evaluation of a P2X7 Receptor-Selective Radiotracer: PET Studies in a Rat Model with Local Overexpression of the Human P2X7 Receptor and in Nonhuman Primates, J Nucl Med, 57 (2016) 1436-1441.
[47] P.R. Territo, J.A. Meyer, J.S. Peters, A.A. Riley, B.P. McCarthy, M. Gao, M. Wang, M.A. Green, Q.H. Zheng, G.D. Hutchins, Characterization Of [11C]-GSK1482160 For Targeting The P2X7 Receptor As A Biomarker For Neuroinflammation, J Nucl Med, (2016).

FIGURE LEGENDS

Figure 1: *Tspo* transcript levels are increased in microglia during pro-inflammatory but not anti-inflammatory signaling.

(a-c) Analysis of transcripts levels by qRT-PCR to validate the pro-inflammatory M1 condition after LPS treatment and the anti-inflammatory M2 state after IL-4 treatment. The typical pro-inflammatory genes *Tnfa* (a) and *iNOS* (b) were only upregulated after LPS treatment and the anti-inflammatory gene *Arg1* (c) was only upregulated in IL4-treated (M2) microglia (d) *Tspo* transcript levels are only significantly increased in M1-activated microglia but not in M2-activated microglia. Data are presented as mean ± SEM (n=3/group). *P < 0.05; ***P < 0.001.

Figure 2: *Tspo* transcript levels remain unchanged after IL-4 i.c.v. injections.

(a-d) With the exception of *iNOS* (b) the expression of typical pro-inflammatory markers *Tnfa* (a), *Il1b* (c) and *Il6* (d) were not altered in the frontal cortex after IL-4 injections in the third ventricle. (e-g) Transcripts levels of anti-inflammatory markers such as *Arg1* (e) and *Fizz1* (f) were markedly increased. The *Ym1* M2 marker was not significantly altered (g). (h) Transcript levels of *Tspo* remain unchanged after IL-4 injections in the third ventricle. Data are presented as mean ± SEM (n=5/group). **P < 0.01; ***P < 0.001.

Figure 3: Widespread increased TSPO transcript and protein levels in *Mfp2*$^{-/-}$ versus control brain predominantly localize in *Mfp2*$^{-/-}$ microglia.

(a) qRT-PCR analysis shows induced *Tspo* transcript levels in brainstem of *Mfp2*$^{-/-}$ mice as compared to age-matched controls at 12 weeks of age. Data are presented as mean ± SEM (n=3/group), **P < 0.01. (b-g) IHC staining shows virtually no immunoreactivity for TSPO (green) in CNS of wild type mice (b-d) but strong upregulation in *Mfp2*$^{-/-}$ brain (e-g), shown for brainstem, colliculus and thalamus. (h,i) IHC of TSPO (green) and Iba1 (red) to mark microglial cells. In healthy brain (h) TSPO levels are minimal so co-localization with Iba1^{+} microglia is not visible. In *Mfp2*$^{-/-}$ mice (i) TSPO immunoreactivity co-localizes with nearly all Iba1^{+} microglia (orange). Merged picture and separate channels for Iba1 and TSPO are shown. (j,k) IHC of TSPO (green) and GFAP (red) to mark astroglia. Astrocytes of control mice (j) minimally express GFAP and TSPO. In CNS of *Mfp2*$^{-/-}$ mice (k) only few GFAP^{+}

reactive astrocytes colocalize with TSPO protein (orange). Merged picture and separate channels for GFAP and TSPO are shown. Representative pictures are shown from colliculus region.

Figure 4: *In vitro* and *ex vivo* autoradiography of brain slices of *Mfp2*$^{-/-}$ and control mice using [^{18}F]DPA-714. (a, b) Sagittal brain sections of *Mfp2*$^{-/-}$ (a) and age-matched control (b) mice were incubated with [^{18}F]DPA-714. Significantly higher uptake is observed in brain sections of *Mfp2*$^{-/-}$ mice. (c,d) [^{18}F]DPA-714 binding was blocked in the presence of 20 µM PK11195 (d). (e-h) Ex vivo autoradiography of sagittal brain sections of *Mfp2*$^{-/-}$ (e,g) and age-matched control (f,h) mice at 30 (e, f) and 60 (g, h) min after [^{18}F]DPA-714 injection. Significantly higher uptake is observed in brain sections of *Mfp2*$^{-/-}$ mice as compared to control at both 30 and 60 min after tracer injection ($P < 0.01$; two-tailed, un-paired student t-test).

Figure 5: MicroPET in *Mfp2*$^{-/-}$ and control mice using [^{18}F]DPA-714.

(a,b) Time activity curves (TACs) expressed as nCi/cc (a) and standard uptake value (SUV g/ml) (b) as a function of time post tracer injection. (c,d) Accompanying brain images of both *Mfp2*$^{-/-}$ and control mice. n =6/group.

Supplementary Figure 1: Confirmation of purity of primary microglia cultures.

Percentage of CD11b positive cells (microglia) in primary cultures after gating for live cells. Data are presented as mean ± SEM (n=3).

Supplementary Figure 2: *Tspo* transcript levels are increased in pro-inflammatory microglia polarized by using IL-1β/IFNγ.

(a-c) Analysis of transcripts levels by qRT-PCR confirms that IL-1β/IFNγ treated (M1) microglia *in vitro* induce expression of typical pro-inflammatory genes such as *Tnfa* (a) and *iNOS* (b) and not the anti-inflammatory gene *Arg1* (c). (d) *Tspo* transcript levels are significantly increased in IL-1β/IFNγ treated (M1) microglia. Data are presented as mean ± SEM (n=4/group). *$P < 0.05$; ***$P < 0.001$.

Supplementary Table: Primer and probe sequences used for qRT-PCR.

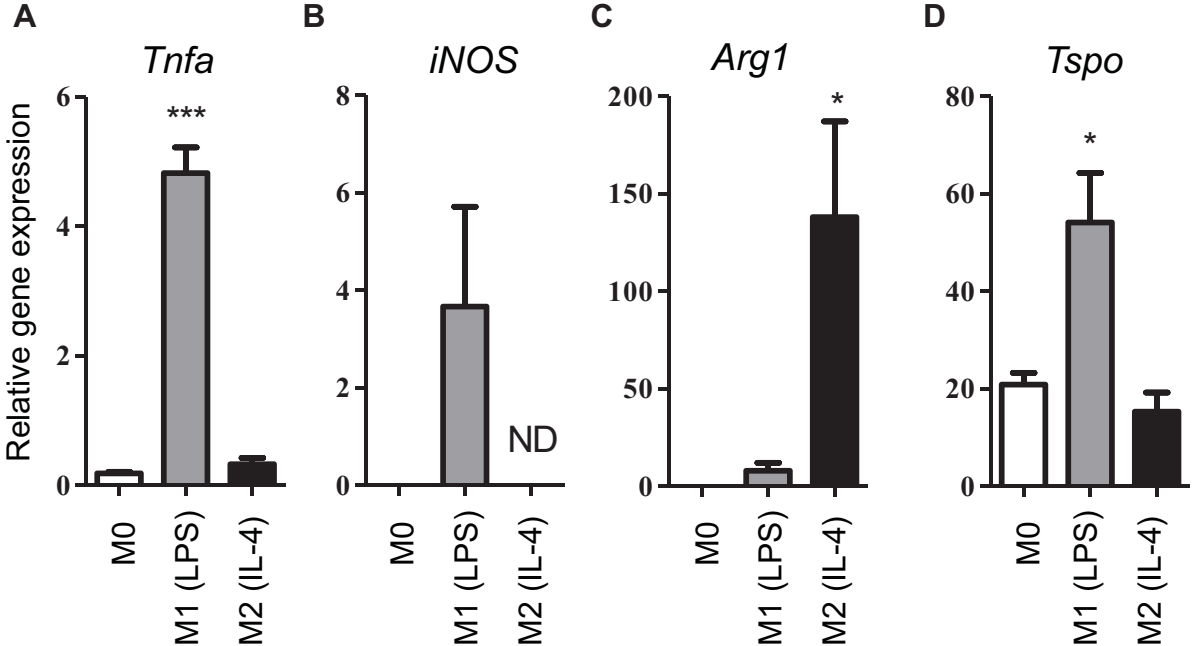
A
Tnfa
Relative gene expression
6
4
2
0
***
M0
M1 (LPS)
M2 (IL-4)
B
iNOS
8
6
4
2
0
ND
M0
M1 (LPS)
M2 (IL-4)
C
Arg1
200
150
100
50
0
*
M0
M1 (LPS)
M2 (IL-4)
D
Tspo
80
60
40
20
0
*
M0
M1 (LPS)
M2 (IL-4)

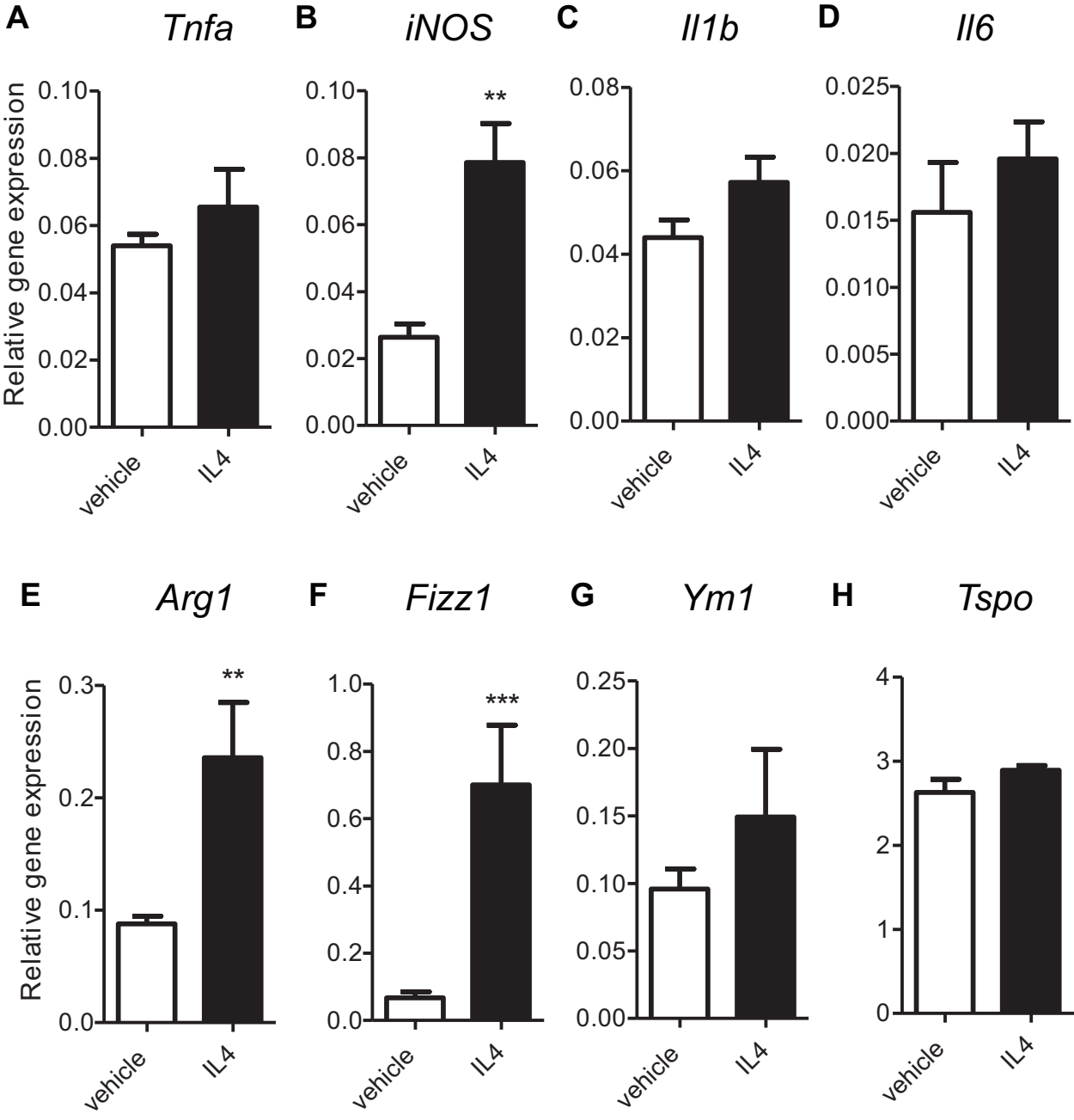
A
Tnfa
B
iNOS
C
Il1b
D
Il6
Relative gene expression
0.10
0.08
0.06
0.04
0.02
0.00
**
0.025
0.020
0.015
0.010
0.005
0.000
vehicle
IL4
E
Arg1
F
Fizz1
G
Ym1
H
Tspo
0.3
0.2
0.1
0.0
1.0
0.8
0.6
0.4
***
0.25
0.20
0.15
0.05
4
3
2
1
0

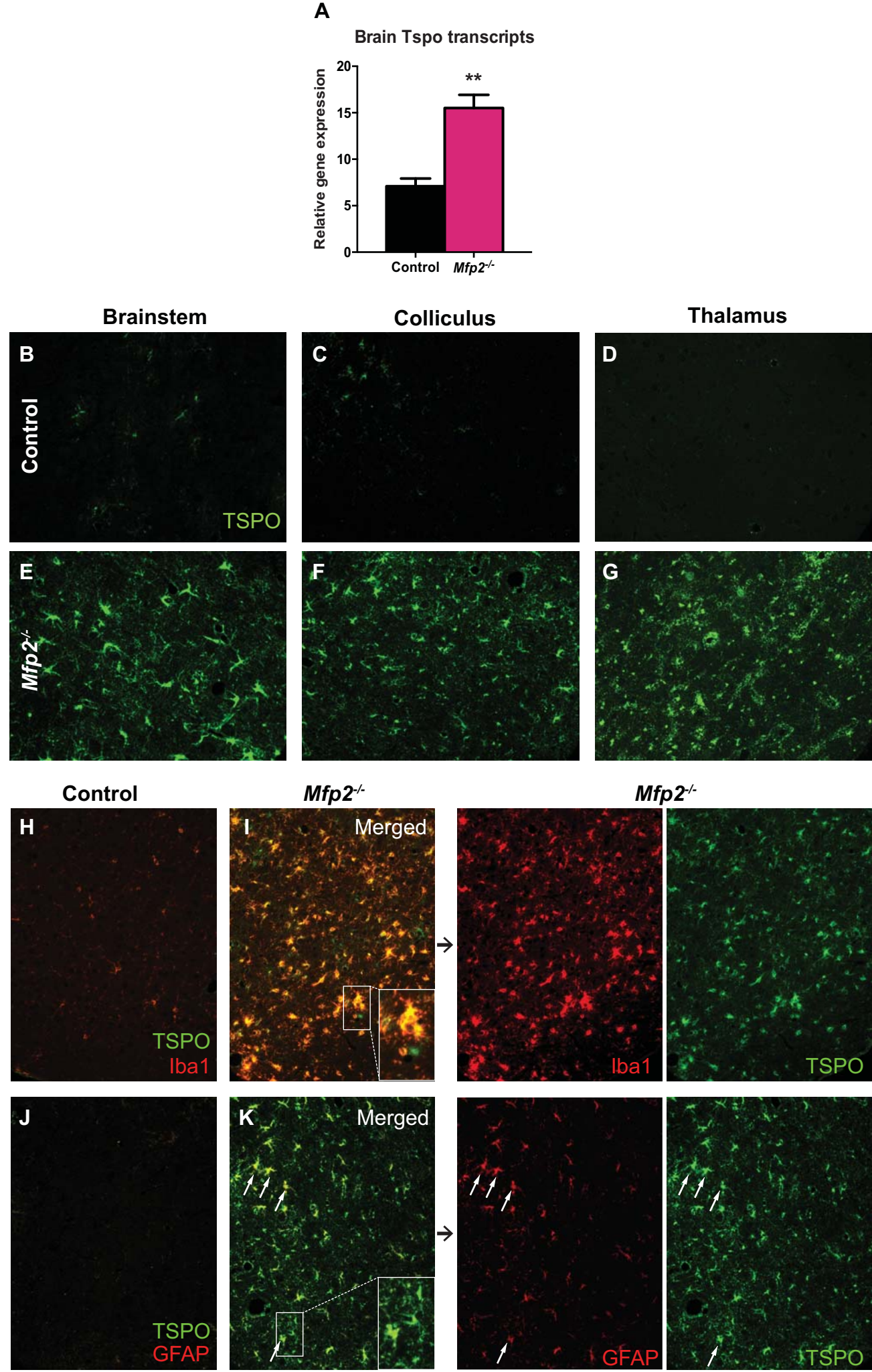
A
Brain Tspo transcripts
Relative gene expression
20
15
10
5
0
**
Control
Mfp2-/-
Brainstem
Colliculus
Thalamus
B
Control
TSPO
C
D
E
Mfp2-/-
F
G
Control
Mfp2-/-
Mfp2-/-
H
TSPO
Iba1
I
Merged
Iba1
TSPO
J
TSPO
GFAP
K
Merged
GFAP
TSPO

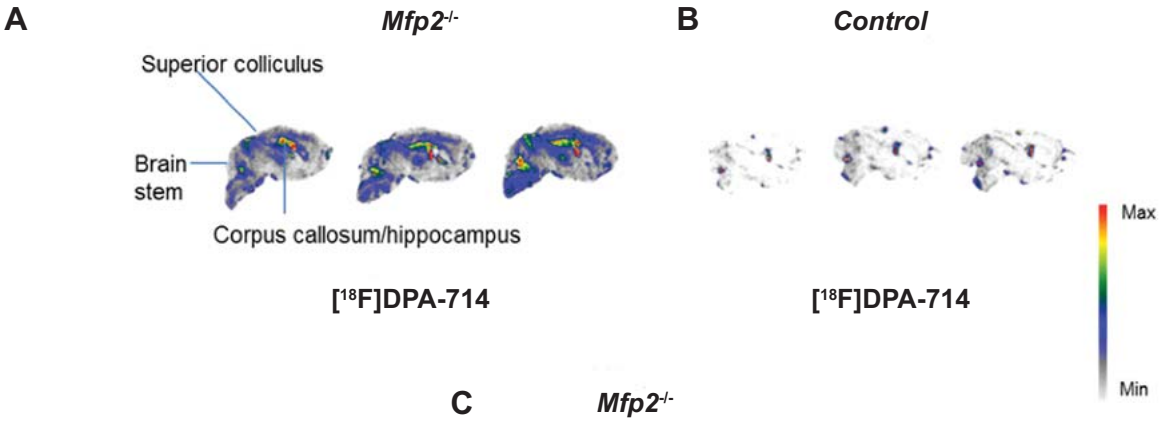
A
Mfp2-/-
Superior colliculus
Brain stem
Corpus callosum/hippocampus
[18F]DPA-714
B
Control
[18F]DPA-714
Max
Min
C
Mfp2-/-
[18F]DPA-714 + 20 uM PK11195
D
Mfp2-/-
30min
E
Control
30min
Max
Min
F
Mfp2-/-
60min
G
Control
60min

Figure 5

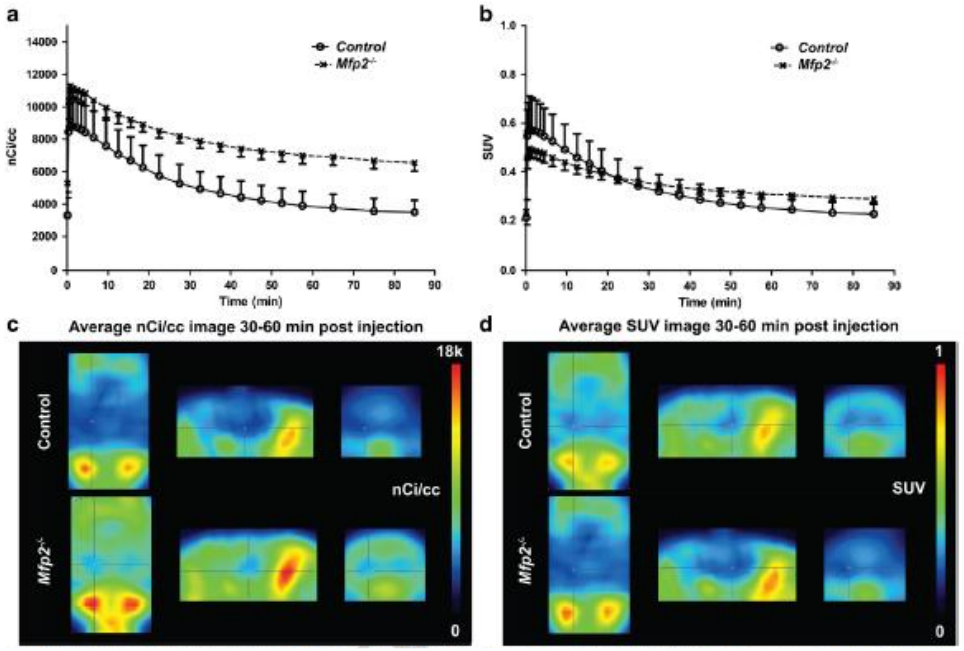
a
Control
Mfp2-/-
nCi/cc
Time (min)
b
Control
Mfp2-/-
SUV
Time (min)
c
Average nCi/cc image 30-60 min post injection
Control
Mfp2-/-
18k
nCi/cc
0
d
Average SUV image 30-60 min post injection
Control
Mfp2-/-
1
SUV
0

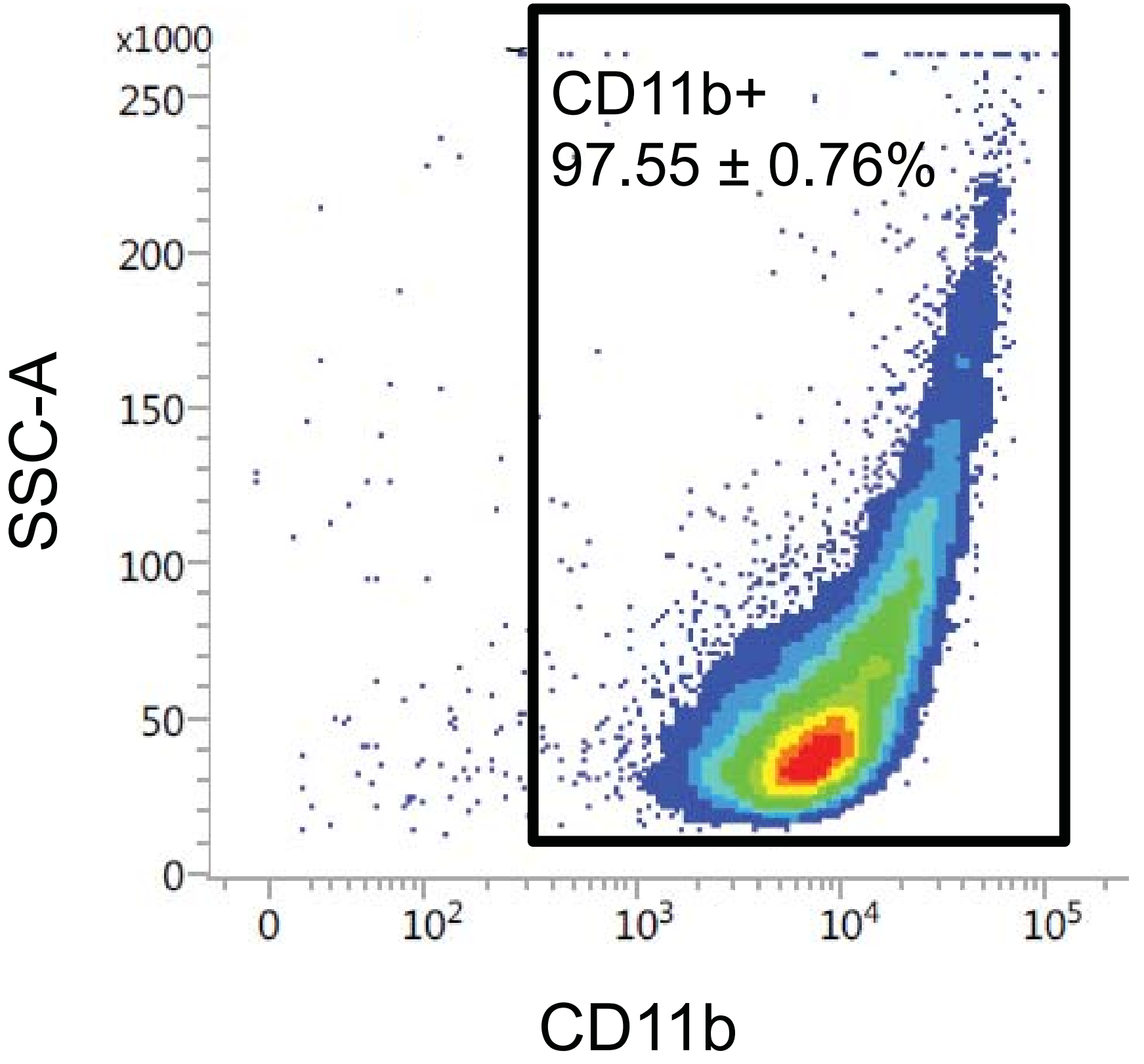
CD11b+
97.55 ± 0.76%
x1000
250
200
150
100
50
0
SSC-A
0
10^2
10^3
10^4
10^5
CD11b

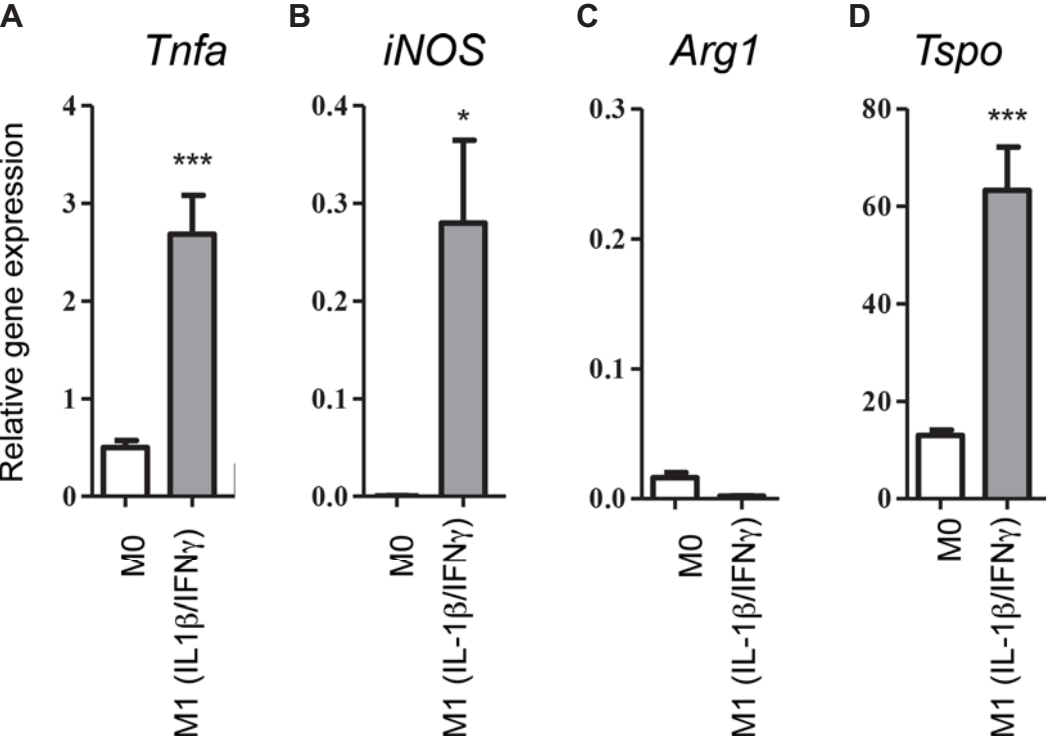
A
Tnfa
B
iNOS
C
Arg1
D
Tspo
Relative gene expression
***
*
***
M0
M1 (IL1β/IFNγ)
M1 (IL-1β/IFNγ)

Gene	Forward	Reverse	Probe
Actb	ATTGGCAACGAGCGGTT	AGGTCTTTACGGATGTCAACG	5'-FAM-ATTCCATACCCAAGAGGAAGGCTGG-TAMRA-3'
TNF	ATCCGCGACGTGGAACTG	ACCGCCTGGAGTTCTGGAA	5'-FAMCAGAAGAGGCACTCCCCCAAAAGATG-TAMRA-3'
iNOS	TGGAGAGATTTGCATGACACTCTT	CCAAGCAAGACTTGGACTTGCA	5'-FAMCACCACAAGGCCACATCGGATTTCACT-TAMRA-3'
Arg1	AAAGGAAAGTTCCCAGATGTACCA	TACGTCTCGCAAGCCAATGTA	5'-FAMTGACTCCCTGCATATCTGCCAAAGACATC-TAMRA-3'
TSPO	GGTTTCACAGAGGACGCTAT	AAGCAGAAGATCGGCCAAG	5'-FAM-AGAGCCAGCTGACCAGTGTAGAGA-TAMRA-3'
Retnla/Fizz1	TGCCAATCCAGCTAACTATCC	CACACCCAGTAGCAGTCATC	5'-FAM-AGGAGGCCCATCTGTTCATAGTCTTGA-TAMRA-3'
Chi3l3/Ym1	AGAAGCAATCCTGAAGACACC	ACTGGTATAGTAGCACATCAGC	5'-FAM-TTGTCACAGGTCTGGCAATTCTTCTGA-TAMRA-3'
Nos2	GGTCCTCTGGTCAAACTCTTG	GATTTTGCATGACACTCTTCACC	5'-FAM-AGGCCACATCGGATTTCACTTGCA-TAMRA-3'
IL1b	TGACAGTGATGAGAATGACCTGTTC	GGACAGCCCAGGTCAQAAGG	5'-FAM-ACCCCAAAAGATGAAGGGCTGCTTCC-TAMRA-3'
IL6	TCCTTAGCCACTCCTTCTGT	AGCCAGAGTCCTTCAGAGA	5'-FAM-CCTACCCCAATTTCCAATGCTCTCCT-TAMRA-3'